Multidisciplinary Journal of Chemistry
Volume 13 Issue 1, January-March 2025
ISSN: 2995-4398
Impact Factor: 9.45
https://kloverjournals.org/index.php/chem

INFRARED MICRO-SPECTROSCOPY AS A DIAGNOSTIC TOOL FOR AMYLOIDOSIS SUBTYPE IDENTIFICATION

Sofia Marie van der Berg
University Medical Center Groningen, Department of Rheumatology & Clinical Immunology, Hanzeplein 1 - 9713 GZ Groningen, Netherlands.
DOI:https://doi.org/10.5281/zenodo.15495491

ABSTRACT: The aim of this study was to assess the use of Synchrotron Radiation Fourier Transform InfraRed micro spectroscopy (SR micro-FTIR) in the diagnosing and subtyping of different misfolded proteins in various tissues and organs. To this end, specimens from various organ sites were investigated. Multivariate data analysis was applied to correlate the spectral datasets with histological and immunohistochemical findings and clinical data. The results of the study reveal significant segregation of tissues affected by amyloidosis and controls, but the observed amount of amyloid β-sheet did not correlate with the disease state. Amyloid light-chain type specimens contained more βsheet structures than non-Amyloid a types, and Tran's thyretrin type showed very little. The Insulin type behaved differently

Keywords: Amyloidosis, Classification, Synchrotron Infrared Micro-Spectroscopy

Introduction

Amyloidosis encompasses a group of disorders caused by protein miss folding in various tissues and organs. There are now over 40 different human amyloid diseases (e.g. Alzheimer's, Parkinson's, Huntington's, prion diseases, type II diabetes, and also some cancers), each linked to a specific soluble precursor protein or peptide. According to (Hopping, Gene, et al, and Sarroukh, Rabia, et al) which can undergo a conformational change that makes it aggregation-prone [1, 2]. The formation of amyloid fibrils involves a transition to β-sheet structure via soluble amyloid genic intermediates which appear to have a molecular geometry distinct from the regular β-sheet. Aggregation is a complex, bidirectional process which may occur via multiple reaction mechanisms, and involves a large number of heterogeneous intermediate [3-6]. Self-seeding 7 and β-sheet structures are not identical in different proteins 8, which further complicates analysis [7, 8]. Routine histopathological diagnostics of amyloid deposits rely on green birefringence of Congo red staining under polarized light. Subtyping is performed by applying specific antibodies against amyloid proteins. The standard immune histo chemical staining can yield equivocal results and can be problematic because of the diversity of proteins present. For instance, approximately 20% of AL amyloid deposits do not stain specifically with antibodies against kappa or lambda immunoglobulin light chain, and therefore the possibility of AL amyloid can be neither excluded nor confirmed by the present immuneohistochemical subtyping. SR miscroFTIR studies have revealed intricate details about the molecular structures of the amyloid fibrils and their precursors in situ and provided insights into the pathways of disease development [9-14]. In association with

Multidisciplinary Journal of Chemistry
Volume 13 Issue 1, January-March 2025
ISSN: 2995-4398
Impact Factor: 9.45
https://kloverjournals.org/index.php/chem

Table 1 Main clinical and histological characteristics of the samples

Controls	System/Organ site
Ctrl GI1	GI/Colon
Ctrl GI2	GI/Gallbladder
Ctrl GI3	GI/Tongue
Ctrl R1	Resp/Lung
Ctrl R2	Resp/Pleura
Ctrl R3	Resp/Voacl Cord
Ctrl S	Skin
Ctrl ST1	Eye/conjuctiva
Ctrl ST2	Conn Tiss
Ctrl ST3	Soft tissue/fat
Ctrl ST4	Soft tissue/syn
Ctrl U1	Urinary/Bladder
Ctrl U1	Urinary/Sem ves

Patient code	System/organ site	Age	Gender	CR	AA	TTR	Kappa/lambda/neg	Local	Summary
GI1	GI/Colon	82	M	pos	neg	neg	lambda	n/a	ALLambda
GI2	GI/Gallbladder	80	M	pos	pos	n/a	n/a	n/a	AA
GI3	GI/Stomach	72	M	pos	neg	Weak	neg	neg	TTR
GI4	GI/Tongue	72	M	pos	neg	n/a	neg	n/a	non AA b2ug
GI5	GI/Tongue	68	F	pos	neg	neg	Kappa	neg	ALSKappa
GI6	GI/Tongue	77	M	pos	neg	neg	Kappa	kappa	AllKappa
LN1	Lymph Node	61	F	pos	neg	neg	neg	n/a	non AA
R1	Resp/Lung	81	M	pos	neg	neg	lambda	n/a	ALLambda
R2	Resp/Lung	65	M	pos	neg	neg	neg	n/a	nonAA
R3	Resp/Lung	82	F	pos	neg	neg	lambda	neg	ALSLambda
R3	Resp/Lung	82	F	pos	neg	neg	lambda	neg	ALSLambda
R3	Resp/Lung	82	F	pos	neg	neg	lambda	neg	ALSLambda
R4	Resp/Lung	72	M	pos	neg	neg	lambda	n/a	ALSLambda
R5	Resp/Pleura	79	M	pos	neg	neg	neg	neg	cr
R6	Resp/Vocal Cord	75	M	pos	neg	neg	Kappa	Kappa	ALLkappa
R7	Resp/Vocal Cord	69	M	pos	neg	neg	neg	n/a	nonAA
S1	Skin	81	M	pos	neg	neg	lambda	neg	ALSLambda
S2	Skin	77	F	pos	n/a	n/a	n/a	n/a	cmd
S3	Skin	67	F	neg	neg	neg	neg	neg	neg
S4	Skin	66	M	weak	n/a	n/a	n/a	n/a	cmd
S5	Skin	66	F	weak	neg	neg	neg	neg	neg
S6	Skin	38	F	pos	neg	neg	neg	neg	cr
S7	Skin	69	M	pos	neg	neg	lambda	n/a	ALSLambda
S8	Skin	65	F	pos	neg	neg	Kappa	Kappa	ALLKappa
E1	Eye/conjuctiva	44	F	pos	neg	neg	lambda	lambda	ALLLambda
E2	Eye/conjuctiva	79	M	pos	neg	neg	Kappa	Kappa	AllKappa
ST1	Soft tissue/fat	50	M	pos	neg	neg	neg	neg	insulin

[3]

multivariate data analysis, SR microFTIR has been used to examine protein miss folding directly within diseased tissue in Alzheimer's disease, Parkinson's disease, Huntington's disease, amyotrophic lateral sclerosis and scrapie [15]. Amyloid fibrils have characteristic amide I bands in the IR spectra, extending from 1611 cm^{-1} to 1630 cm^{-1}, whereas native intermolecular βsheet protein structures produce amide I peaks clustering between 1630 cm^{-1} and 1643 cm^{-1} [16]. Ami et al, used the 1630 cm^{-1} component in the amide I band and the associated 1531 cm^{-1} component in the Amide II band as characteristic markers for the AL amyloid deposits in human tissues [17]. However, rare forms of amyloidosis have not been extensively studied and we are aiming to exploit SR microFTIR sensitivity to identify and subtype different amyloid proteins in various organs and tissues and understand if the type and degree of variations can be attributable to the tissue of origin and type of misfolded protein.

MATERIALS AND METHODS Collection and Preparation of Material Human tissues were acquired from patients during biopsy examination for diagnostic purposes. There were 24 male and 9 female patients with

Average age at diagnosis of 74 years for males and 63 years for female patients (Table 1).

ST2	Soft tissue/fat	82	M	pos	neg	neg	neg	neg	non AA
St3	Soft tissue/ret	69	M	pos	neg	pos	neg	neg	TTR
ST4	Soft tissue/syn	80	M	pos	neg	pos	neg	neg	TTR
U1	Urinary/Bladder	73	M	pos	neg	pos	neg	neg	TTR
U2	Urinary/Bladder	73	M	pos	neg	neg	Lambda	neg	ALLambda
U3	Urinary/Bladder	77	M	pos	neg	neg	Kappa	neg	ALSKappa
U4	Urinary/Bladder	88	M	pos	neg	pos	neg	neg	TTR
U5	Urinary/S.Ves	59	M	pos	neg	pos	staining	neg	TTR

Note: The patients were grouped according to the system and organ involved and by type of amyloid protein detected. GI- gastrointestinal tract, R -respiratory, Urinary-Urinary tract, S. ves- Seminal Vesicles; CR-Congo Red, AA-Amyloid A, TTR- Transthyretin, b2μg- deposited protein is β2 microglobulin; Ins - deposited protein is Insulin, n/d- no data, n/a- non applicable, Summary column-cr-congo red positive only, AL-type of amyloidosis where deposited protein is either kappa or lambda light immunoglobulin chain; AL can be systemic (ALS) or local (ALL). In case there was no data if systemic or local, designation AL was left, nonAA - amyloid of non-AA type (amyloid deposits which do not stain with antibodies against kappa or lambda immunoglobulin light chain), neg- cases that failed to show expression of any of the proteins, crnd-cases that were positive on histochemical stain for amyloidosis but were negative for immunohistochemical subtyping, neg- cases that failed to show expression of any of the stains applied. Amyloid-negative tissues used as a control are acquired from resection margins of excised malignancies or from biopsies that resulted negative for inflammation, dysplasia or malignancy on histological examination. For SR-microFTIR analysis, samples were cut from tissue blocks; microtomed 4 μm thick sections of tissue were floated onto 2 mm thick UV-grade CaF_2 windows (Crystran Ltd., Dorset, UK) for transmission mode FTIR microspectroscopy. The sections were dewaxed by immersion in xylene (5 min, twice) and then washed in a series of ethanol/water (100% x2, 95%, and 80% to remove the xylene). In clearly labelled Petri dishes, the sections are then put in a warm chamber to facilitate the removal of atmospheric water. In addition, previous and succeeding adjacent slices have been cut onto standard glass slides to perform Haematoxylin and Eosin (H and E) staining for conventional histology. 8 μm thick sections were used for Congo Red (CR) staining and was performed using the automatic staining protocol for the Ventana Benchmark Ultra platform using the modified Highman method and amyloid was identified by the presence of apple green birefringence when viewed under crossed polarised light. 3 μm tissue sections were sectioned on TOMO slides for immunohistochemical staining. The stainings were performed using the automatic staining protocols for the Ventana Benchmark Ultra platform (Roche Diagnostics, Almere, and the Netherlands). Used antibodies derived from Agilent (San Clara, CA, USA) were a

monoclonal antibody against AA (clone mc1) and polyclonal antibodies against kappa, lambda, and Transthyretin (TTR) at dilutions of 1: 3200, 1: 16000, 1: 16000, and 1: 6400, respectively. For AA, pre-treatment was done with Protease while the standard Ultra CC1 pre-treatment was done for the other antibodies. The detection was done with the standard method of the Ultra system.

SR-FTIR Measurements

All FTIR imaging data were collected at the MIRIAM beamline B22 at the Diamond Light Source UK synchrotron facility. The measurements were performed using Bruker Vertex 80V Vacuum-FTIR interferometer coupled with the fully automated Hyperion 3000 microscope with liquid nitrogen-cooled MCT detector.

2024 13(1):

IR windows were mounted on the motorised XY stage of the microscope and the sample was located using the 36x objective, a map of the sample was created and saved using the integrated CCD camera, and around 80 points/sample (from 50-100) were chosen before commencing data acquisition [18]. The spectra were collected in transmission mode to avoid artefacts and to facilitate the results of interpretation. Selected areas were mapped focusing the SR IR beam at the sample plane within 10 μm^2 x10 μm^2 slits apertures and 36 x Schwarzschild objective and a matching condenser ((N.A. 0.63), optimizing signal on the broadband 50 μm MCT detector in the background (CaF_2), and cumulating 256 scans (velocity 80 kHz, spectral resolution 4 cm^{-1}) within the 4000 cm^{-1}-650 cm^{-1} interval to obtain acceptable S/N values). A background reading was taken after every 10 points. The estimated time to acquire the spectrum of a spot area of 10 μm^2 x 10 μm^2 was 30 seconds. Data was recorded using OPUS 7.5 software (Bruker Optik GmbH, Ettlingen, Germany) [19].The spectra and their associated metadata were exported from the Bruker system and were analysed in R 4.1 with the PLS and MASS packages [20-22]. The spectra were baseline-corrected to zero offset at 1800 cm^{-1} and then normalised to the Amide I band. First derivative spectra were calculated by direct difference, using a 5-point offset for minimal smoothing. Initial analyses with the whole IR spectrum showed strong signal interference in the region from 3000 cm^{-1}-2800 cm^{-1} from residual paraffin, whose strong aliphatic CH bands could not be removed completely. To exclude this and other interference such as the CO_2 bands, the spectral region from 3000 cm^{-1}-2000 cm^{-1} was excluded from the analysis. Multivariate models were made with the first derivative spectra and resulting loadings vectors corresponded to first derivatives spectra had to be integrated to be better interpretable. Partial Least Squares (PLS) regression was done against nominal values as described in the text. The Root Mean Square Error of Prediction (RMSEP) values reached a minimum with 10-12 components. For consistency, all PLS models were made with 10 components. Leave-one-out internal cross validation was employed throughout. Training and test sets were selected by specimen as described in the text.

Method Development

Spectral feature selection and data pre-treatment: The infrared spectra of the tissue sections were dominated by the protein bands: Amide A at 3500 cm^{-1}-3100 cm^{-1}, Amide I at 1700 cm^{-1}-1600 cm^{-1}, Amide II from 1560 cm^{-1}-1490 cm^{-1}, and Amide III at 1300 cm^{-1}-1200 cm^{-1}. Also notable were strong

and very sharp aliphatic C-H bands in the 3000 cm^{-1}-2850 cm^{-1} region and a concomitant doublet of small bands at 1450 cm^{-1} and 1460 cm^{-1}. These bands are most certainly from remnants of the paraffin wax of the original biopsy blocks, but their intensities were not reproducible. That would indicate some differences in the preparation process between the tissue series. The various washes with ethanol and xylene during the dew axing process would remove most, but perhaps not all the paraffin, and may also remove other soluble compounds and affect some protein secondary structures. Tissue preparation is potentially the largest sources of artefacts and must always be kept in mind when interpreting data [23, 24]. The variable CO_2 bands at ~2300 cm^{-1} should also be ignored. Below 1100 cm^{-1} the spectra quality deteriorated markedly due to the optical setup of the system and the CaF_2 sample carriers. Therefore, the spectral regions from 3600 cm^{-1} -3000 cm^{-1} and 2000 cm^{-1}-1100 cm^{-1} were used for making the PLS models. SR infrared spectra are prone to distortion by Mie scattering, but the use of PLS with first derivative spectra seemed to avoid it affecting the models and the PLS loadings showed rather random residues of background distortion [25, 26]. Model validation: The accepted measure of quality for PLS models are the Root Mean Square Error of Prediction (RMSEP) with unrelated test samples. The sections came from a range of different types and cases with few or no matching replicates. The variability between specimens could be due to their different origins, but even with closely matched samples, the averages varied slightly. More significantly, in each specimen, the spectra had a distinct spread of ratios. The large number of point spectra measured with each section can give a good approximation of that particular specimen, but they were not truly independent because section thickness, treatment history, scattering, etc. could all affect the spectra band shapes in a non-random way. Because of the potential correlation within specimens the conventional way of validating the PLS models by dividing the spectra randomly in a calibration set and a test set would not be appropriate. To establish robust predictive models, the sample selection for calibration and validation was done on the specimen level. All PLS models were made using 10 components because the Root Mean Square Error of Calibration (RMSEC) only reached a minimum with about 10-12 components. This slow decrease signalled that the correlation between the spectra variations and the modelled property was rather complex. Although the first three components discussed in the text were the strongest, they did only cover between 37% (Resp. model) and 92% (Skin model) of the whole variability (Figure 1). Moreover, the datasets contained a lot of unrelated variations which would impair the quality of the models. Using so many components obviously improved the predictions, but on the other hand it did increase the risk of overfitting. Nevertheless, it was remarkable how well the models could identify amyloidosis, given that the spectra from some of the case specimens looked exactly like controls and did not show any sign of the amyloid structures.

			Amide band ratio	**Tissue models**	**Type models vs controls**	**Type models vs cases**

Multidisciplinary Journal of Chemistry
Volume 13 Issue 1, January-March 2025
ISSN: 2995-4398
Impact Factor: 9.45
https://kloverjournals.org/index.php/chem

Patient c	oSystem/organ si	n_spectr	ratio (SD)		GI tract (SD)		Respiratory tract		Skin (SD)		Soft tissue (SD)		Urinary tract (SD)		AL (SD)		non AA (SD)		TTR (SD)		INS (SD)		AL case (SD)		non AA case (SD)		TTR case (SD)		INS case (SD)	
Ctrl GI1	GI/Colon	70	0.81	(0.03)	0.00	(0.09)	0.24	(0.06)	0.79	(0.07)	0.56	(0.06)	0.78	(0.08)	0.21	(0.09)	0.04	(0.06)	0.04	(0.06)	0.01	(0.03)	0.42	(0.14)	0.24	(0.09)	0.25	(0.09)	0.08	(0.02)
Ctrl GI2	GI/Gallbladder	71	0.79	(0.04)	0.02	(0.07)	0.21	(0.08)	0.84	(0.09)	0.52	(0.09)	0.62	(0.11)	0.18	(0.07)	0.09	(0.08)	0.12	(0.08)	-0.03	(0.03)	0.16	(0.13)	0.37	(0.08)	0.44	(0.09)	0.01	(0.03)
Ctrl GI3	GI/Tongue	92	0.71	(0.03)	0.12	(0.07)	0.23	(0.06)	0.87	(0.03)	0.66	(0.05)	0.69	(0.07)	0.23	(0.07)	0.20	(0.04)	0.23	(0.06)	0.07	(0.03)	0.21	(0.08)	0.30	(0.06)	0.39	(0.12)	0.07	(0.02)
GI1	GI/Colon	91	0.79	(0.03)	1.00	(0.08)	0.77	(0.09)	1.09	(0.04)	0.87	(0.04)	0.94	(0.04)	0.76	(0.08)	0.71	(0.07)	0.88	(0.08)	0.22	(0.11)	0.58	(0.06)	0.14	(0.06)	0.30	(0.10)	0.00	(0.04)
GI2	GI/Gallbladder	91	0.80	(0.02)	0.96	(0.05)	0.68	(0.04)	1.03	(0.04)	0.87	(0.04)	0.92	(0.05)	0.67	(0.05)	0.65	(0.04)	0.82	(0.07)	0.27	(0.12)	0.59	(0.12)	0.13	(0.06)	0.32	(0.06)	-0.01	(0.03)
GI3	GI/Stomach	86	0.84	(0.04)	0.97	(0.10)	0.59	(0.08)	0.93	(0.11)	0.70	(0.12)	1.02	(0.10)	0.61	(0.10)	0.63	(0.07)	0.86	(0.09)	0.08	(0.16)	0.35	(0.15)	0.15	(0.09)	0.55	(0.12)	0.01	(0.03)
GI4	GI/Tongue	104	0.61	(0.03)	0.96	(0.04)	0.27	(0.21)	1.04	(0.03)	0.96	(0.04)	1.03	(0.04)	0.55	(0.04)	0.88	(0.05)	0.82	(0.07)	0.07	(0.06)	0.11	(0.11)	0.59	(0.28)	0.27	(0.04)	-0.02	(0.03)
GI5	GI/Tongue	89	0.83	(0.05)	0.89	(0.06)	0.68	(0.08)	1.09	(0.06)	0.83	(0.07)	0.94	(0.05)	0.71	(0.06)	0.62	(0.05)	0.75	(0.14)	0.25	(0.09)	0.53	(0.12)	0.12	(0.07)	0.30	(0.16)	0.03	(0.02)
GI6	GI/Tongue	70	0.80	(0.04)	1.01	(0.05)	0.80	(0.09)	1.17	(0.06)	1.00	(0.10)	0.96	(0.09)	0.79	(0.05)	0.72	(0.05)	0.92	(0.08)	0.42	(0.06)	0.58	(0.10)	0.09	(0.08)	0.24	(0.15)	0.09	(0.02)

LN1	Lymph Node	71	1.12	(0.09)	0.47	(0.09)	0.84	(0.08)	0.75	(0.05)	0.46	(0.07)	0.51	(0.06)	0.59	(0.09)	0.87	(0.10)	0.18	(0.12)	0.09	(0.04)	0.19	(0.09)	0.89	(0.16)	-0.21	(0.15)	-0.01	(0.03)
Ctrl R1	Resp/Lung	77	0.98	(0.10)	0.27	(0.09)	0.10	(0.11)	0.81	(0.08)	0.47	(0.05)	0.88	(0.08)	0.24	(0.09)	0.07	(0.07)	0.03	(0.08)	0.01	(0.03)	0.45	(0.09)	0.26	(0.08)	0.17	(0.07)	0.05	(0.03)
Ctrl R2	Resp/Pleura	71	0.79	(0.04)	0.07	(0.13)	0.08	(0.07)	0.63	(0.08)	0.29	(0.10)	0.47	(0.06)	0.09	(0.13)	0.12	(0.06)	0.11	(0.05)	0.05	(0.02)	-0.01	(0.15)	0.51	(0.10)	0.47	(0.05)	0.00	(0.02)
Ctrl R3	Resp/Vocal Cord	70	0.72	(0.01)	0.13	(0.05)	0.13	(0.05)	0.84	(0.05)	0.54	(0.03)	0.68	(0.04)	0.20	(0.05)	0.13	(0.03)	0.27	(0.03)	0.03	(0.02)	0.14	(0.08)	0.24	(0.05)	0.60	(0.04)	0.02	(0.02)
R1	Resp/Lung	100	1.08	(0.10)	1.17	(0.14)	1.02	(0.11)	0.97	(0.11)	0.88	(0.12)	0.96	(0.17)	0.93	(0.14)	0.89	(0.17)	0.91	(0.12)	0.28	(0.19)	0.66	(0.17)	0.21	(0.18)	0.16	(0.15)	-0.03	(0.04)
R2	Resp/Lung	94	1.14	(0.11)	1.19	(0.19)	1.01	(0.11)	1.04	(0.06)	0.81	(0.03)	0.98	(0.05)	1.01	(0.19)	1.04	(0.11)	0.84	(0.08)	0.17	(0.12)	0.24	(0.09)	0.71	(0.14)	-0.01	(0.12)	0.00	(0.02)
R3	Resp/Lung	56	0.78	(0.03)	1.08	(0.17)	1.01	(0.04)	1.01	(0.05)	1.03	(0.05)	1.08	(0.16)	1.00	(0.17)	0.72	(0.11)	1.03	(0.10)	0.36	(0.14)	0.91	(0.08)	-0.04	(0.08)	0.11	(0.08)	0.02	(0.03)
R3	Resp/Lung	56	0.78	(0.02)	1.10	(0.10)	1.00	(0.05)	1.03	(0.05)	1.01	(0.04)	1.05	(0.11)	0.94	(0.10)	0.74	(0.13)	1.02	(0.10)	0.42	(0.18)	0.89	(0.10)	-0.02	(0.06)	0.08	(0.07)	0.03	(0.02)
R3	Resp/Lung	60	1.16	(0.03)	1.20	(0.04)	0.98	(0.05)	1.11	(0.04)	0.81	(0.03)	1.22	(0.06)	1.09	(0.04)	1.19	(0.05)	0.85	(0.06)	0.24	(0.14)	0.73	(0.06)	0.22	(0.06)	0.05	(0.04)	-0.02	(0.01)
R4	Resp/Lung	77	1.03	(0.12)	0.56	(0.11)	0.92	(0.13)	0.82	(0.07)	0.69	(0.06)	0.71	(0.11)	0.88	(0.11)	0.79	(0.18)	0.34	(0.11)	0.18	(0.07)	0.92	(0.16)	0.26	(0.08)	-0.	(0.06)	-0.	(0.02)

																										20		05	
R5	Resp/Pleura	63	0.95	(0.04)	1.25	(0.10)	1.00	(0.10)	1.15	(0.03)	0.87	(0.06)	0.94	(0.09)	0.93	(0.10)	0.88	(0.08)	0.94	(0.05)	0.35	(0.10)	0.77	(0.06)	0.00	(0.07)	0.24	(0.10)	-0.02	(0.03)
R6	Resp/Vocal Cord	58	0.99	(0.09)	1.25	(0.17)	0.92	(0.04)	1.21	(0.06)	1.05	(0.05)	1.24	(0.09)	1.04	(0.17)	1.03	(0.15)	1.08	(0.11)	0.45	(0.05)	0.85	(0.10)	-0.07	(0.07)	0.23	(0.06)	0.03	(0.02)
R7	Resp/Vocal Cord	89	0.87	(0.09)	0.86	(0.12)	0.83	(0.10)	1.04	(0.06)	0.80	(0.10)	1.02	(0.10)	0.66	(0.12)	0.84	(0.10)	0.80	(0.09)	0.25	(0.13)	0.34	(0.10)	0.22	(0.09)	0.32	(0.16)	0.05	(0.03)
Ctrl S	Skin	71	0.83	(0.03)	0.11	(0.13)	0.15	(0.07)	0.14	(0.12)	0.11	(0.10)	0.40	(0.13)	0.04	(0.13)	0.07	(0.07)	0.03	(0.05)	0.00	(0.05)	0.13	(0.17)	0.55	(0.12)	0.33	(0.08)	-0.10	(0.03)
S1	Skin	63	1.05	(0.27)	1.74	(0.05)	1.34	(0.33)	1.05	(0.05)	1.34	(0.05)	1.48	(0.05)	1.22	(0.05)	1.36	(0.05)	1.62	(0.05)	0.55	(0.13)	0.83	(0.25)	-0.04	(0.08)	0.20	(0.05)	0.05	(0.03)
S2	Skin	109	0.89	(0.06)	0.88	(0.10)	0.74	(0.14)	0.97	(0.07)	0.84	(0.09)	0.84	(0.11)	0.66	(0.10)	0.63	(0.06)	0.77	(0.11)	0.24	(0.15)	0.61	(0.14)	0.09	(0.16)	0.26	(0.12)	-0.01	(0.03)
S3	Skin	65	0.78	(0.10)	0.94	(0.08)	0.52	(0.23)	0.99	(0.06)	0.82	(0.07)	0.89	(0.23)	0.64	(0.08)	0.86	(0.13)	0.81	(0.18)	0.20	(0.12)	0.24	(0.19)	0.46	(0.14)	0.24	(0.18)	-0.04	(0.04)
S4	Skin	77	0.97	(0.08)	0.92	(0.07)	0.83	(0.20)	0.98	(0.03)	0.75	(0.10)	1.07	(0.08)	0.78	(0.07)	0.82	(0.10)	0.87	(0.11)	0.36	(0.09)	0.36	(0.13)	0.23	(0.09)	0.33	(0.07)	0.08	(0.02)
S5	Skin	118	0.79	(0.18)	0.81	(0.06)	0.52	(0.46)	0.98	(0.03)	0.84	(0.21)	0.95	(0.06)	0.57	(0.06)	0.86	(0.07)	0.61	(0.10)	0.26	(0.25)	0.16	(0.18)	0.65	(0.27)	0.07	(0.07)	-0.04	(0.03)

S6	Skin	80	0.82	(0.04)	0.91	(0.08)	0.59	(0.06)	0.95	(0.07)	0.79	(0.09)	0.90	(0.12)	0.63	(0.08)	0.77	(0.08)	0.89	(0.03)	0.27	(0.06)	0.35	(0.09)	0.19	(0.04)	0.51	(0.04)	-0.04	(0.02)
S7	Skin	66	1.08	(0.05)	0.99	(0.05)	0.91	(0.06)	1.03	(0.04)	0.77	(0.04)	1.19	(0.10)	0.93	(0.05)	1.12	(0.13)	0.80	(0.06)	0.25	(0.10)	0.89	(0.16)	-0.02	(0.06)	0.14	(0.07)	0.02	(0.02)
S8	Skin	72	1.02	(0.07)	0.49	(0.13)	0.61	(0.05)	0.96	(0.05)	0.68	(0.05)	0.66	(0.08)	0.57	(0.13)	0.31	(0.06)	0.26	(0.07)	0.03	(0.05)	0.69	(0.09)	0.20	(0.05)	0.20	(0.06)	-0.03	(0.03)
Ctrl ST1	Eye/conjuctiva	71	0.80	(0.03)	0.27	(0.19)	0.28	(0.10)	0.71	(0.21)	0.17	(0.17)	0.57	(0.12)	0.21	(0.19)	0.12	(0.11)	0.17	(0.14)	0.00	(0.04)	0.27	(0.22)	0.29	(0.10)	0.45	(0.13)	-0.07	(0.03)
Ctrl ST2	Conn Tiss	70	0.82	(0.06)	0.17	(0.15)	0.08	(0.07)	0.62	(0.07)	0.19	(0.09)	0.59	(0.13)	0.08	(0.15)	0.01	(0.06)	0.03	(0.06)	-0.01	(0.04)	0.16	(0.20)	0.36	(0.13)	0.48	(0.12)	-0.01	(0.06)
Ctrl ST3	Soft tissue/fat	83	1.01	(0.13)	0.03	(0.27)	-0.12	(0.23)	0.58	(0.25)	0.07	(0.17)	0.65	(0.21)	-0.13	(0.27)	-0.04	(0.13)	-0.08	(0.20)	0.00	(0.06)	0.04	(0.32)	0.54	(0.16)	0.28	(0.17)	0.04	(0.03)
Ctrl ST4	Soft tissue/syn	56	0.76	(0.02)	-0.09	(0.08)	0.13	(0.07)	0.51	(0.12)	0.04	(0.06)	0.46	(0.07)	0.05	(0.08)	0.01	(0.08)	-0.09	(0.12)	-0.01	(0.03)	0.21	(0.11)	0.32	(0.08)	0.39	(0.09)	0.00	(0.03)
E1	Eye/conjuctiva	60	0.96	(0.11)	0.99	(0.12)	0.75	(0.14)	1.02	(0.10)	1.03	(0.14)	0.75	(0.13)	0.80	(0.12)	0.74	(0.14)	0.98	(0.15)	0.47	(0.11)	0.61	(0.15)	0.08	(0.11)	0.23	(0.13)	0.09	(0.04)
E2	Eye/Conjuctiva	112	1.21	(0.06)	1.19	(0.07)	1.15	(0.11)	0.96	(0.05)	0.97	(0.06)	1.48	(0.15)	1.01	(0.07)	1.40	(0.17)	1.06	(0.07)	0.38	(0.17)	0.77	(0.12)	0.12	(0.07)	0.14	(0.10)	0.02	(0.05)
ST1	Soft tissue/fat	57	1.00	(0.20)	0.99	(0.20)	0.94	(0.26)	1.25	(0.15)	1.00	(0.10)	1.35	(0.33)	1.06	(0.20)	0.99	(0.39)	1.09	(0.30)	0.87	(0.26)	0.16	(0.21)	0.15	(0.08)	0.17	(0.20)	0.43	(0.20)

ST2	Soft tissue/fat	70	0.92	(0.10)	0.43	(0.28)	0.27	(0.18)	0.87	(0.19)	0.65	(0.17)	0.74	(0.17)	0.49	(0.28)	0.53	(0.26)	0.28	(0.12)	0.14	(0.06)	0.06	(0.08)	0.54	(0.08)	0.14	(0.13)	0.08	(0.05)
ST3	Soft tissue/ret	93	0.72	(0.01)	0.53	(0.04)	0.28	(0.03)	0.93	(0.02)	0.90	(0.04)	0.75	(0.04)	0.36	(0.04)	0.46	(0.04)	0.82	(0.03)	0.21	(0.05)	0.16	(0.05)	0.08	(0.04)	0.79	(0.07)	0.03	(0.01)
ST4	Soft tissue/syn	81	0.83	(0.04)	0.98	(0.12)	0.87	(0.11)	1.14	(0.05)	0.88	(0.06)	0.98	(0.12)	0.77	(0.12)	0.72	(0.06)	0.96	(0.12)	0.40	(0.16)	0.48	(0.13)	0.09	(0.07)	0.43	(0.13)	0.02	(0.03)
Ctrl U1	Urinary/Bladder	51	0.84	(0.04)	0.02	(0.19)	0.16	(0.13)	0.64	(0.11)	0.43	(0.12)	0.13	(0.13)	0.15	(0.19)	-0.02	(0.07)	-0.06	(0.12)	-0.02	(0.03)	0.32	(0.24)	0.37	(0.15)	0.30	(0.08)	-0.02	(0.06)
Ctrl U2	Urinary/Semves	70	0.77	(0.01)	0.04	(0.05)	0.77	(0.06)	0.88	(0.03)	0.75	(0.05)	0.04	(0.06)	0.09	(0.05)	0.00	(0.04)	-0.04	(0.05)	0.01	(0.01)	0.75	(0.07)	0.11	(0.03)	0.25	(0.11)	-0.10	(0.02)
U1	Urinary/Bladder	98	0.79	(0.06)	0.88	(0.12)	0.48	(0.11)	0.98	(0.06)	0.81	(0.07)	0.98	(0.07)	0.58	(0.12)	0.61	(0.06)	0.91	(0.07)	0.21	(0.10)	0.25	(0.10)	0.19	(0.08)	0.56	(0.08)	0.01	(0.03)
U2	Urinary/Bladder	90	0.76	(0.02)	0.74	(0.07)	0.52	(0.06)	0.95	(0.03)	0.74	(0.04)	0.98	(0.04)	0.50	(0.07)	0.62	(0.03)	0.78	(0.04)	0.27	(0.08)	0.27	(0.07)	0.19	(0.04)	0.53	(0.07)	0.03	(0.02)
U3	Urinary/Bladder	70	1.15	(0.05)	1.06	(0.20)	0.90	(0.08)	1.14	(0.08)	0.76	(0.08)	0.96	(0.08)	1.05	(0.20)	0.88	(0.21)	0.62	(0.21)	0.34	(0.06)	1.16	(0.11)	-0.14	(0.06)	0.04	(0.08)	-0.04	(0.03)
U4	urinary/Bladder	70	0.77	(0.03)	0.15	(0.10)	0.31	(0.11)	0.71	(0.11)	0.30	(0.11)	0.95	(0.10)	0.75	(0.10)	-0.05	(0.08)	-0.13	(0.11)	-0.09	(0.06)	0.80	(0.15)	0.07	(0.07)	0.05	(0.15)	0.03	(0.04)
U5	Urinary/S. Ves	90	0.99	(0.10)	0.87	(0.08)	0.95	(0.11)	1.12	(0.05)	1.07	(0.05)	1.00	(0.05)	0.77	(0.08)	0.83	(0.10)	0.92	(0.12)	0.20	(0.16)	0.47	(0.11)	0.08	(0.06)	0.56	(0.14)	0.02	(0.03)

Figure 1 The PLS predictions for all specimens with the different models. Each value in the table is the average of all n spectra in the section. The first coloured data column shows the 1630 cm^{-1}/1655 cm^{-1} intensity ratio for comparison

RESULT

We analysed 33 Formalin Fixed Paraffin-Embedded (FFPE) specimens from the following sites: lung (4), tongue (3), vocal cord (2), bladder (4), soft tissue (5), gallbladder (1), seminal vesicles (1), stomach (1), pleura (1), skin (8), conjunctiva (2), colon (1). Respective controls were also included (Table 1). There were 18 cases of AL (in 4 of 18 subtyping permitted exclusion of AA type deposit but could not demonstrate AL which is reported to be the case in ~20% of AL deposits, these cases were called non-AA subtype), 6 cases of Transthyretin (TTR), 1 β-2 microglobulin, 1 case of Insulin (Ins) deposition, 3 cases where subtyping was negative on all proteins tested and positive only for Congo red stain. 1 case where even Congo red on repeated sections turned out to be negative, and 3 cases where subtyping was not possible for the paucity of material. Figure 2 shows the staining in light micrographs of some of these specimens, indicating the patchy deposition of aggregated proteins.

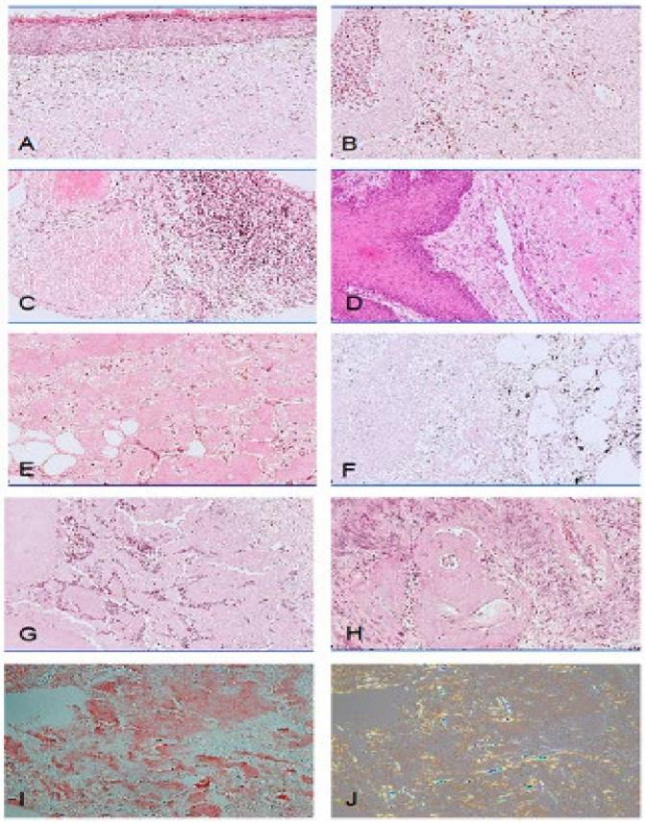

Figure 2 Microphotograph of amyloid deposits; routine histochemical Haematoxylin and Eosin (H&E) stain in skin (A), bladder mucosa (B), conjunctiva of the eye (C), tongue (D), soft tissues (E), lung (F), seminal vesicles (G) and vasculature of the stomach infiltrated by Gastrointestinal Stromal Tumours (GIST, H). Amyloid deposits are highlighted by Congo red histochemical stain (I) and are seen as a pale green birefringence under polarised light (J)

Multidisciplinary Journal of Chemistry
Volume 13 Issue 1, January-March 2025
ISSN: 2995-4398
Impact Factor: 9.45
https://kloverjournals.org/index.php/chem

The defining feature of AL amyloid deposits is their characteristic intermolecular β-sheet structure [17]. Most tissues contain a large portion of α-helical proteins, so the build-up of amyloid deposits with their characteristic β-sheet absorption is expected to change the shapes of the amide bands in the infrared spectra from the affected regions compared to those from healthy tissue. Amide A at ~3300 cm^{-1}, Amide I at ~1650 cm^{-1}, Amide II at ~1550 cm^{-1} and Amide III at around 1300 cm^{-1}-1200 cm^{-1} are all sensitive to the protein secondary structures [18,19].

Figure 3 compares the approximate ratio of β-sheet to α-helix indicated by the amide I band intensities at 1630 cm^{-1} and 1655 cm^{-1} in the IR spectra of each specimen. There were some differences between controls from different tissues: the ratio was 0.71 in Ctrl G3, 0.72 in Ctrl R3, and 0.76 in Ctrl ST4. The spectra from these sections showed a relatively small variation of the ratio and the amide I bands had peak positions around 1650 cm^{-1}-1655 cm^{-1} characteristic for predominantly α-helical protein structures [18]. However, two control specimens CtrlR1 and Ctrl ST3 had ratios around 1, due to more β-sheet content, and the spectra of these specimens also had a considerably larger variability, indicating that these samples were much less homogeneous. The average ratio in the remaining controls was typically around 0.8.

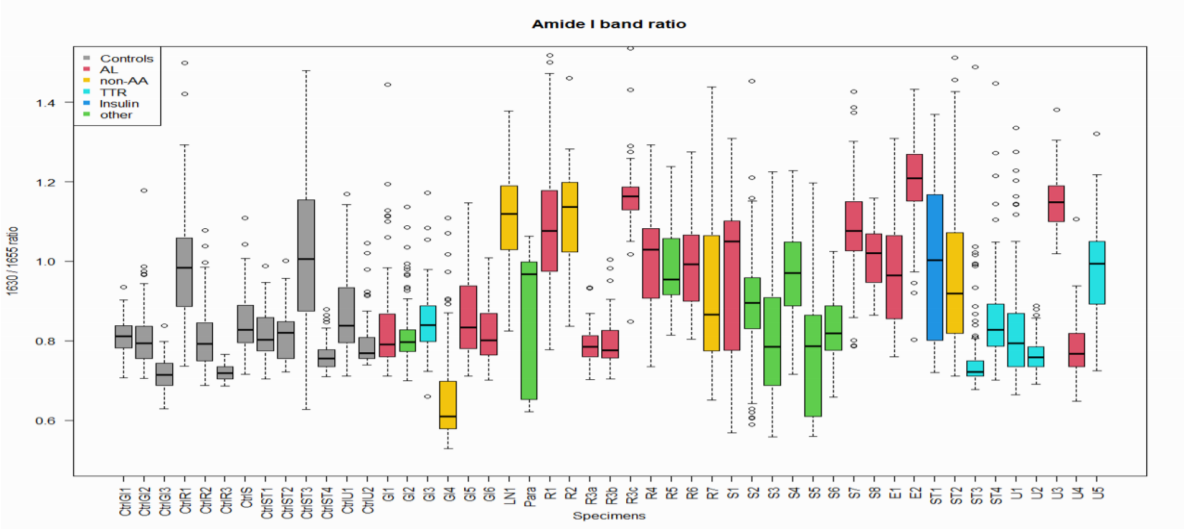

Figure 3 Ratios of the 1630 cm^{-1}/1655 cm^{-1} intensities in the IR spectra. Each boxplot represents a specimen and is coloured by the amyloidosis subtype. The whiskers indicate the spread of values for the spectra in each specimen

In the amyloid case samples, the AL lambda subtype tended to have a very strong effect in most tissues except in the GI tract specimens, with a ratio above 1, and a shift of the amide I band maximum down to 1634 cm^{-1}-1638 cm^{-1}. AL kappa on the other hand only had such strong shifts in the skin specimens. In the other tissues the change was much less pronounced or not visible at all. The Ins ST/fat case specimen with amyloidosis due to insulin deposition had a value of 1. TTR showed a strong shift in the soft tissue specimen only, but not in the GI tract or Urinary system specimens. NonAA subtype showed a pronounced signal from amyloid structures in the respiratory tract specimens, but not in the soft

tissue or the GI tract. Generally, the GI tract seemed to be less affected than the other tissues, and the respiratory system the most. Thus, in our data set the band shapes varied widely both with amyloid type/subtype and tissue. While many specimens showed the expected increase in the Amide band I component at 1630 cm^{-1} and the associated 1531 cm^{-1} component in the Amide II band, in many other case specimens the IR spectra looked almost identical to those of the controls [17]. Obviously, there was no consistent correlation between the amounts of β-sheet structures and the disease state.

Tissue-Type Specific Amyloidosis Models

To compare the impact of amyloidosis in different organs, the specimens were grouped into five tissue systems: Respiratory Tract (resp), containing lung, pleura and vocal cord tissue, Gi Tract (GI), containing tongue, stomach, gallbladder and colonic mucosa, Soft Tissue (ST), containing conjunctival soft tissue, abdominal fat, retinaculorum and synovium, Skin (skin), and Urinary System (Uro), containing bladder and seminal vesicles.

Comparison of the original IR spectra (Supplementary figure SF2 and supplementary table ST1) hinted at the variation **2024 13(1):** Within specimens in the tissues. Principal Component Analysis (PCA) (Supplementary figure SF3) mostly did not separate cases from controls and did not consistently distinguish between amyloid subtypes. PCA picks out variance in the spectra, which can be due to any number of factors. The PCA loadings indicated a strong contribution from the amide bands, but the spectra did contain other variability, in the baseline, the paraffin bands, and also different noise levels. Section thickness, treatment, sample mounting, can have an effect as well as different protein structures. In contrast, Partial Least Squares (PLS) regression extracts variance that is correlated with observations/sample values. In this particular model setup, the controls had been assigned the value 0 and cases the value 1, and this model was not designed to distinguish between subtypes. Using PLS in this way has the advantage of giving a numeric value related to similarity rather than simply group membership. The PLS model loadings can also give an idea which spectral features were correlated with the transition from healthy to the disease state. The models were made with the first derivative of the two spectra regions 3800 cm^{-1}-3100 cm^{-1} and 1900 cm^{-1}-1100 cm^{-1}. Consequently, the model loadings and coefficients contained sinusoidal first-derivative features. To aid with the interpretation, the loadings were integrated to re-gain recognisable IR bands in the figures. The PLS predictions for all specimens with the different models are listed in Figure 1. Figure 4 shows the integrated first three PLS loadings for the control vs disease PLS models in the five tissue systems.

Multidisciplinary Journal of Chemistry
Volume 13 Issue 1, January-March 2025
ISSN: 2995-4398
Impact Factor: 9.45
https://kloverjournals.org/index.php/chem

Figure 4 Integrated loadings from the tissue specific amyloidosis PLS models using the selected Amide A/B and Amide I/II/III regions,
Loading 1, loading 2, and loading 3
024 13(1):

Gastrointestinal tract: The GI tract cases vs GI controls PLS model performed very well. The GI calibration sample fits were close to the nominal values 0 for controls, 1 for cases. In GI tract, we have a specimen from colonic mucosa, gallbladder, and tongue and so called Gastrointestinal Stromal Tumour (GIST) of the stomach. The latter shows amyloidosis only in the wall of blood vessels, so the shifts found here may not be organ specific. This was also the case in colonic mucosa where the deposits were exclusively vascular. When the model was applied to the other tissues, all controls were assigned low values, and cases were assigned high ones. The only exception was U3 (Urinary/Bladder ALSKappa), which was assigned a similarly low value, and also had the same amide I band ratio, as a control. All other case predictions were clearly higher than any control, but there was a group of specimens in the test cases with values hovering around 0.5. However, at this stage the values could not be attributed unambiguously to the subtypes or locations of the amyloid deposits because the samples were mostly from single specimens and differences between the case specimens could be due to sample variation. The first loading of the GI PLS model relating to the largest correlated compound, showed positive bands at 3268 cm^{-1} in the amide A region, 1649 (shoulder) and 1610 cm^{-1} in the amide I, at 1516 cm^{-1} in the amide II and at 1222 cm^{-1} in the amide III region. It also had negative bands at 3336 cm^{-1}, 1669 cm^{-1}, 1554 cm^{-1}, and 1245 cm^{-1}. The changes in the Amide I and II band regions are very similar to the pattern identified by Ami et al. [17]. Therefore, this loading would represent loss of native α-helix, random, and turn structure and increase in the amyloid βsheet. Other changes in the tissue are

indicated by the higher loadings. A feature to note is a change in the Amide a band region around 3300 cm^{-1}. All five tissue models had a positive band at 3280 cm^{-1} associated with the amyloid β-structure, and there was a negative band around 3330 cm^{-1} associated with native (helical etc.) structure. Overall, there was a strong indication that the Amide A band experienced a characteristic shift towards lower wavenumbers, whose extent varied between the tissue systems. The Amide a band is generally not thought to be influenced by the backbone structure, only by hydrogen bonding strength. However, Krimm and Bandekar reported shifts as large as 40 cm^{-1} between different sheet structures [19]. Moreover, the bands observed in the PLS models are well-defined and quite distinct from the wide baseline variations. Therefore, it would be reasonable to consider them as specific markers in addition to the patterns seen in the Amide I and II band region.

Respiratory system: The Resp. cases vs Resp. controls model performed almost as good. Controls and case specimens were clearly distinguished. The three Resp control specimens, which originated in different organs lung, pleurum, and vocal cord were close, but had slightly different average values. The Resp. calibration specimens had all average values close to 1 as expected. The spectra from R4 had a remarkably wider spread of values than those from the other lung samples. This could be patient specific, but without having more samples to confirm this, variations in the averages and in the spread of the values were most likely due to the sampling and preparation of individual sections. When this Resp model was applied to the other tissues, the average assigned values for the 'unknown' controls was somewhat higher than the Resp controls, and one Uro/SemVes control came out as suspect with a value of 0.77. The case sample values were mostly between 0.5 and 1, lower than the Resp calibration samples, but still higher than the controls. However, four specimens (G4, ST2, ST3, and U4), had low values that could have them classed as false negatives if a case diagnosis were made based on the output of this PLS model. The first loading of the Resp PLS model showed strong positive peaks at 3280 cm^{-1}, 1615 cm^{-1}, 1540 cm^{-1}-1510 cm^{-1}, and 1220 cm^{-1}, indicating an increase in amyloid β-sheet structure. Only the third loading showed clear negative bands at 3315 cm^{-1}, 1648 cm^{-1}, 1540 cm^{-1} and 1240 cm^{-1} relating to the loss of native helical structures. This strong emphasis on amyloid deposition could explain why specimens with low amide I ratio were generally fitted with lower PLS values.

Skin: The Skin cases vs Skin control model was probably skewed by the fact that there was only a single control specimen in the calibration. This PLS model had a big gap between the skin control and the skin case values. Perhaps that was not surprising, because skin specimens had some of the most extreme shifts in the amide bands. When applied to the other tissues, this model gave rather high values for all controls other than skin. However, the case sample values were also higher throughout. There were only three case samples (LN1, R4 and U4) with values similar to the controls. On the whole, it would seem that this model separated reasonably well between controls and cases, albeit with a shifted boundary. The Skin PLS model basis appeared quite different from the others the first loading showed negative peaks at 3340, 1660 cm^{-1}, 1563 cm^{-1}, 1460 cm^{-1}, 1238 cm^{-1} and 1205 cm^{-1}, and positive bands only at 3275 cm^{-1} and 1620 cm^{-1} (small). The second loading had positive bands at 3335 cm^{-1}, negative at 1652 cm^{-1}, 1610 cm^{-1} and 1545 cm^{-1}. The third loading had negative bands at 3289 cm^{-1}, 1635 cm^{-1},

1564 cm^{-1}, but positive at 1230 cm^{-1}. The skin specimens were mostly ill defined (cr, neg) and had lower amide I ratios. These band changes could therefore relate to tissue damage in those cases, rather than a defined deposition of amyloid.

Soft tissue: The four calibration controls from conjunctival soft tissue, connective tissue, abdominal fat and synovium varied slightly, but again, those were single specimens, so it could not be attributed to organ origin. The figure 1 specimen (conjunctival soft tissue ALLkappa) had a markedly lower average than the other cases and overlapped with the controls. All other calibration specimens were well separated from the controls. However, while the calibration controls and samples were assigned well, the distinction between controls and cases was less clear when this model was applied to the other tissues. The averages for controls were around 0.5 and the cases around 0.8, with considerable overlaps when taking into consideration the distribution of values within each specimen.

The first loading of the ST PLS model showed similarly strong positive bands at 3285 cm^{-1}, 1620 cm^{-1}, 1515 cm^{-1}, and 1225 cm^{-1} related to deposition of amyloid as the Resp model. The second loading had negative bands at 3315, 1658(sh) cm^{-1}, 1615 cm^{-1}, 1520 cm^{-1}, and 1245 cm^{-1}. This model seemed to detect changes in inter and intramolecular β-sheet structures but was less accurate with differentiating between controls and cases.

Urinary tract: The two control specimens behaved quite differently, and the PLS model indicated that the Urinary/bladder specimen (Ctrl U1) spectra showed a particularly widespread of values. All three Uro TTR specimens were tightly grouped around similar average values, and there was no suggestion of one behaving differently. ALLambda and ALSkappa Uro specimens had more variety. Again, the PLS model did clearly separate all calibration cases from the calibration controls, but it did not work as well when applied to other tissues. While case samples did show broadly higher values than controls, there was a large overlap; many case specimens would count as false negatives, and even some controls as false positives.

The first loading of the Uro PLS model had a positive peak at 3267 cm^{-1}, and a sharp peak at 1627 cm^{-1} and broad 1516 cm^{-1} and weak 1231 cm^{-1} peak. The second and third loadings also showed sharp peaks in the Amide I/II band regions. Like the soft tissue model, the Urinary tract model assigned the calibration controls and samples well but made a poor distinction between unknown controls and cases.Taken together, these results showed a strong dependence of the model performance on the calibration samples. While the first two tissue-based PLS models correctly assigned unknown samples from other tissues, the latter three models had problems. The case values were generally higher than controls, but the gap between controls and cases was smaller and the variability much higher.

Type-Specific Amyloidosis Models

PLS models for AL (both lambda and kappa), nonAA, and TTR and INS cases versus all controls were made to find characteristics of these amyloidosis types across the tissues. The model predictions are listed in Figure 1. Figure 5 shows the integrated first three PLS loadings for the type vs control PLS models.

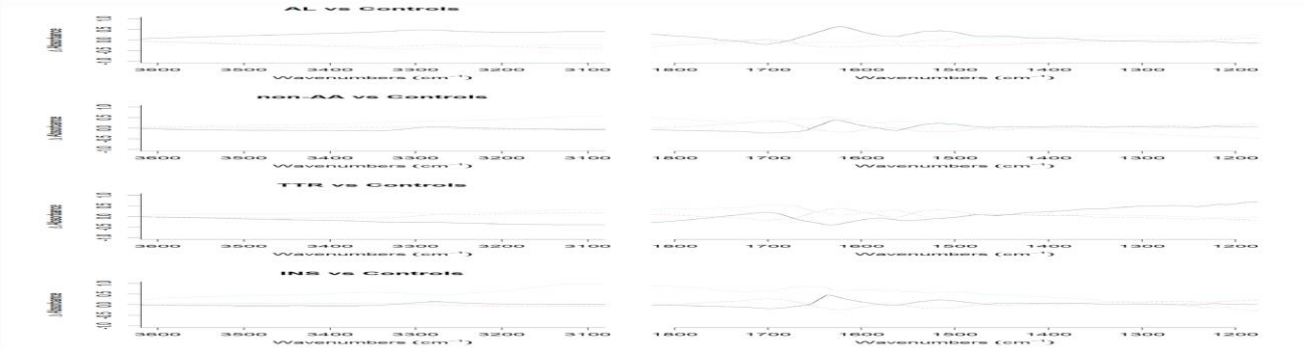

Figure 5. Integrated loadings from the PLS models for the AL, non-AA, TTR and INS amyloid types vs controls. Loading 1, loading 2, and loading 3

AL: The AL calibration samples had fitted PLS between 0.57 and 1.4. However, the other case samples were also assigned relatively high values, higher than the controls (-0.13 to 0.24) and spanning a similar range than the AL samples. The first loading in AL/ctrl model had strong positive bands at 3285 cm^{-1}, 1618 cm^{-1}, 1520 cm^{-1} and 1227 cm^{-1} and indicated the deposition of β-sheet structures. The second loading had neg/pos feature at 3334/3270 cm^{-1}, broad negative bands at 1655 cm^{-1}-1610 cm^{-1} and 1530 cm^{-1}-10 cm^{-1}. The third loading showed negative bands at 3310 cm^{-1}, 1655 cm^{-1}, 1610, cm^{-1} 1545 cm^{-1} and 1242 cm^{-1}.

Both these related to the loss of native, predominantly helical structures, and seemed to be more important with the control/case distinction than the variable amounts of β-sheet. Thus, this model did separate amyloid cases and controls, but could not distinguish AL from other types.

NonAA: The nonAA vs controls PLS model performed similar to AL. The controls had values around 0, but all case specimens except U4 had high values, so there was no separation at all between the nonAA and other types. The loadings were similar to the ones form the AL model. The first loading Non-AA/ctrl model showed strong positive bands at 3273 cm^{-1} (neg 3338), 1631 cm^{-1}, 1515 cm^{-1} and 1222 cm^{-1}. The second loading had positive amide A region band at 3285 cm^{-1}, broad negative amide bands at 1620 cm^{-1}, 1535 cm^{-1}-1510 cm-^{1}, and 1236 cm^{-1}. The third loading was indistinct in the Amide A region, but had positive bands at 1670 cm^{-1}, 1627 cm^{-1} and 1555 cm^{-1}. The positions were slightly different as AL, but the pattern was the same: the first loading related to β-sheet structures, whereas the other two indicated the loss of native structure. TTR: The TTR vs controls model assigned a few more case specimens (LN1, R4, S7, U4) similarly low values as the controls, but most test specimens fell in same range as the TTR specimens, so there was again no clear separation of TTR from other types. The first loading of the TTR/ctrl model had negative peaks at 3324 cm^{-1}, 1628 cm^{-1} (1660 sh), 1545 cm^{-1} and 1240 cm^{-1}. The second loading showed positive peaks at 3270 cm^{-1}, 1618 cm^{-1}, 1509 cm^{-1} and 1233 cm^{-1}. The third loading had positive bands at 3345 cm^{-1}, and 1700 cm^{-1}-1670 cm^{-1}, negative at 3266 cm^{-1}, 1615 cm^{-1}, 1510 cm^{-1} and 1223 cm^{-1}. This inversion reflected the observation that the amide I ratios of the TTR specimens were as low as or even lower than the controls. Nevertheless, the model did not separate TTR from other types with higher amide I ratios, which again indicated that the amount of amyloid deposit was irrelevant for this kind of model.

Insulin: The Insulin vs controls model was the only PLS model that did separate the INS type from the other amyloid types. Two case specimens (S8 and U4) were close to 0, in the same range as the controls, but the majority ranged from 0.17 to 0.55, markedly lower than the 0.87 of the Ins. The problem with this model was that there was only this single INS specimen for calibration, and therefore the model cannot be considered reliable. The bands in the INS/ ctrl model were sharper than in the previous models, perhaps indicating a better-defined deposit: The first loading showed strong positive peaks at 3275 cm^{-1}, 1630 cm^{-1}, 1511 cm^{-1} and 1221 cm^{-1}. Loading 2 had a positive peak at 3329 but negative peaks at 1622 cm^{-1}, 1510 cm^{-1} and 1226 cm^{-1}. The third loading was pos/neg at 3350/3286 cm^{-1}. It had a positive band at 1660 cm^{-1}.

Direct Comparison of Types in Amyloidosis Cases

The previously described AL, nonAA and TTR models with controls as references all tended to assign unknown specimens as cases. The model loadings exhibited similar spectral features to the tissue-type models. Therefore, these models were influenced by common changes from healthy to disease state, rather than by amyloid type. To establish more specific discriminators, PLS models were made for the AL (both lambda and kappa), nonAA, TTR and INS types against all characterised cases. The model predictions are listed in Figure 1. Figure 6 shows the integrated first three PLS loadings for the type versus all cases of PLS models.

Multidisciplinary Journal of Chemistry
Volume 13 Issue 1, January-March 2025
ISSN: 2995-4398
Impact Factor: 9.45
https://kloverjournals.org/index.php/chem

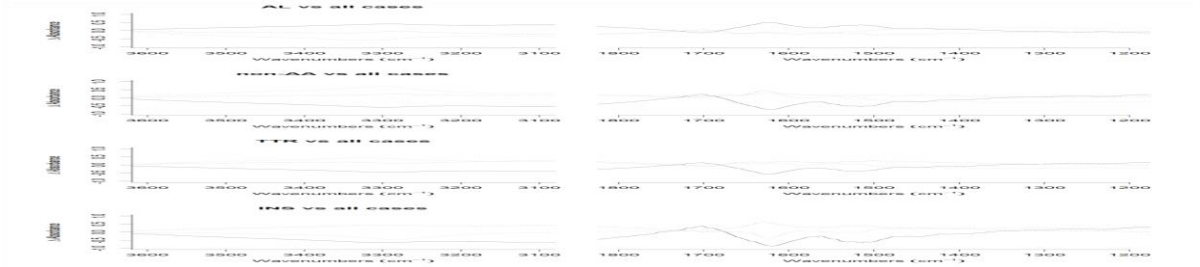

Figure 6. Integrated loadings from the PLS models for the AL, non-AA, TTR and INS amyloid types vs confirmed cases. Loading 1, loading 2, and loading 3

AL cases: The fitted values from this model clearly distinguished between AL type and the other type cases. The fitted values of NonAA, TTR and INS specimens were lower. The control samples, which had not been included in the model calibration, returned also low values, except for Ctrl U2. When this AL cases model was applied to the poorly characterised specimens (cr, nd etc.), three (GI2, R5, S2) fell in the same range as the AL cases, the other four were much lower. The first two loadings in the AL/cases model indicated changes in the inter/intramolecular β-sheet structures. Loading 1 had positive peaks at 3290 cm^{-1}, 1616 cm^{-1}, 1511 cm^{-1}, and 1222 cm^{-1}. Loading 2 was positive at 3278 cm^{-1}, negative at 1649 cm^{-1}, 1504 cm^{-1}, 1236 cm^{-1}. Only loading 3 had negative peaks at 3321 cm^{-1}, 1656 cm^{-1}, 1616 cm^{-1}, 1560 cm^{-1}, 1238 cm^{-1} which related to α-helical structures.

Non-AA cases: The nonAA model performed erratically. One of the nonAA calibration samples (R7) was fitted a low value consistent with the other amyloid types. From the unassigned test cases, S3 and S5 and some of the controls had similar values as the non-AA specimens. The erratic behaviour may be because different proteins may fall into this very vague nonAA category, we know very little about nonAA and what really makes this group of exclusion. In the nonAA/cases model loading 1 showed negative peaks at 3294 cm^{-1}, 1619 cm^{-1}, 1515 cm^{-1}, 1227 cm^{-1} due to changes in βsheet. nonAA specimens had mostly lower amide I ratios than the AL. Loading 2 had positive bands at 3276 cm^{-1}, and 1627 (sharp) cm^{-1}. Loading 3 had positive peaks at 3291 cm^{-1}, 1617 cm^{-1}, and 1545 cm^{-1} -1515 cm^{-1}.

TTR cases: The TTR model also separated TTR cases from the other type cases, with consistently higher PLS values than the other specimens. It fitted all test cases except S6 similarly low values. However, the control sample values ranged rather widely, some had equally high values as the TTR specimens.

Loading 1 in the TTR/cases model had negative peaks at 3287 cm^{-1}, 1622 cm^{-1}, 1517 cm^{-1}, and 1226 cm^{-1}. As with nonAA, TTR had mostly lower amide I ratios than AL. Loading 2 was negative at 3278 cm^{-1}, and positive at 1649 cm^{-1}, 1605 cm^{-1},
1510 cm^{-1}, and 1236 cm^{-1}. Loading 3 had positive bands at 3317 cm^{-1}, 1650 cm^{-1}, 1608 cm^{-1}, 1540 cm^{-1}, 1515 cm^{-1}, and 1227 cm^{-1}.

INS type: In the Ins model only the INS specimen had a large value (0.43), all other case and control sample values were around 0. Loading 1 of the INS / cases model had strong negative peaks at 3295 cm^{-1}, 1616 cm^{-1}, 1515 cm^{-1}, and 1220 cm^{-1}, showing comparatively less β-sheet than the other case

specimens in the calibration set. Loading 2 had positive peaks at 3283 cm^{-1}, 1626 cm^{-1}, 1522 cm^{-1}, and 1230 cm^{-1}. Loading 3 had strong negative peaks at 3285 cm^{-1}, 1621 cm^{-1}, 1541 cm^{-1} and 1249 cm^{-1}. Both were quite distinct. However, as mentioned before, there was only a single INS specimen for calibration, and therefore the model cannot be considered reliable.

Poorly Characterised Samples

The sample set contained six samples (R5, S2, S3, S4, S5, and S6) whose subtype was not defined. Only R5 and S4 showed elevated amide I band ratios, but all six specimens were denoted as amyloid cases by the GI tract case model. R5 and S2 scored high in the AL type model, S3 and S5 scored high in the nonAA type model, S4 and in particular S6 scored high with the TTR type model. None showed any similarity with Ins.

DISCUSSION

The measurement positions on the case specimens had been matched to visual morphology and protein deposits shown by the Congo red staining. Thus, the case spectra represented essentially the diseased state. However, the IR spectra showed that the amounts of β-sheet structures varied widely from specimen to specimen, which indicated clearly that the amount of deposited amyloid protein was not the defining factor for the disease state. The PLS prediction values did not strongly correlate with the amide ratios either and the case assignment was apparently due to other factors than the amount of deposited amyloid protein. It is likely that the correlation was based on spectral features induced by morphological changes in the tissues, and these could arguably be more representative of the disease state than the actual amount of deposited protein. This fits with the current hypothesis that the damage is actually caused by misfolded precursors, and the amyloid deposition is a secondary effect, whose extent may depend on location and patient history. The precursors are likely transient and may not accumulate in sufficient amounts to impact the IR spectra on their own but cause significant changes in the tissues which could be picked up with infrared spectroscopy. The tissue models showed quite distinct behaviours and were based on different spectral band patterns. However, the distribution of amyloidosis types was not even across the tissues. The GI model did perform well across the whole tissue range, which indicated that there was a common set of parameters to predict amyloidosis in all tissues. In contrast, other models which emphasised the AL deposits or special features were much less successful. In spite of the different performance of the five models, many case specimens were assigned consistently high values, and a number of samples (LN1, R4, S8, ST2, ST3, U4) were assigned consistently low values in several models. Therefore, the impact of amyloidosis must be considered more important for the calibration than the location of the deposits. The AL, nonAA and TTR models vs the controls behaved very similar, despite being based on different case samples with widely varying amounts of amyloid deposits. These three models all separated cases from controls but did not distinguish amyloid types. This strongly suggests that the predominant factor in these models was not protein deposition, but changes related to cell/tissue damage. Only the INS models with its very narrow distinct bands did behave differently, but it had only one sample, so it cannot be generalised. The models of amyloid type against the defined cases revealed clear differences between the amyloid typed

nonAA, TTR and INS had less amyloid deposits than AL, and the secondary protein changes were different.

CONCLUSION

The data set and models in this work were purely exploratory, but they demonstrated that the IR spectra contained relevant information about the amyloid disease. More evolved models with suitable large calibration sets could be utilised as diagnostics tool and help to assign cases with insufficient immuno-histological staining.

ACKNOWLEDGEMENTS

We acknowledge Diamond Light Source for time on Beamline 22 under Proposal SM20216 and SM23458.

We acknowledge The University Medical Center Groningen, Amyloidosis Center of Expertise and the Department of Pathology, for help with the subtyping of amyloid deposits. Quadram Institute Biosciences receives strategic funding from BBSRC UK.

Many thanks to the family of Mr Bruno and to Mr Verga for availability, help and support. Their contribution was crucial for the study."

REFERENCES

Hopping, Gene, et al. "Designed α-sheet peptides inhibit amyloid formation by targeting toxic oligomers." Elife 3, 2014.

Sarroukh, Rabia, et al. "ATR-FTIR: A “rejuvenated” tool to investigate amyloid proteins." Biochimica et Biophysica Acta (BBA)-Biomembranes, Vol. 10 ,1828, 2013, pp. 2328-38.

Bi, Timothy M., and Valerie Daggett. "Focus: medical technology: the role of α-sheet in amyloid oligomer aggregation and toxicity." The Yale Journal of Biology and Medicine, Vol. 91, No. 3, 2018, pp. 247.

Childers, Matthew Carter, and Valerie Daggett. "Drivers of α-sheet formation in transthyretin under amyloidogenic conditions." Biochemistry,Vol. 58, No. 44, 2019,pp. 4408-23.

Childers, Matthew C., and Valerie Daggett. "Edge strand dissociation and conformational changes in transthyretin under amyloidogenic conditions." Biophysical Journal, Vol. 119, No.10, 2020, pp. 1995-2009.

Shea, Dylan, et al. "α-Sheet secondary structure in amyloid β-peptide drives aggregation and toxicity in Alzheimer’s disease." Proceedings of the National Academy of Sciences, Vol. 116, No. 18, 2019, pp. 8895-8900.

Surmacz-Chwedoruk, Weronika, et al. "The emergence of superstructural order in insulin amyloid fibrils upon multiple rounds of self-seeding." Scientific Reports, Vol. 6, No. 1, 2016, pp. 320-22